NANO LETTERS

pubs.acs.org/NanoLett Letter

Visualization of the Final Stage of Sintering in Nanoceramics with Atomic Resolution

Tanna Elyn Rodrigues Fiuza, Marlon Muniz da Silva, Jefferson Bettini, and Edson Roberto Leite*

Cite This: https://doi.org/10.1021/acs.nanolett.1c04708 Read Online

ACCESS | Metrics & More | Article Recommendations | Supporting Information

ABSTRACT: The deep understanding of the sintering mechanism is pivotal to optimizing denser ceramics production. Although several models explain the sintering satisfactorily on the micrometric scale, the extrapolation for nanostructured systems is not trivial. Aiming to provide additional information about the particularities of the sintering at the nanoscale, we performed in situ experiments using high-resolution transmission electron microscopy (HRTEM). We studied the pore elimination process in a ZrO_2 thin film and identified a high anisotropic pore elimination. Interestingly, there is a redistribution of the atoms from the rough surface in the solid−gas surface, followed by the atom attachment in a faceted surface. Finally, we found evidence of the pore acting as a pin, reducing the GB mobility. These findings certainly can contribute to enhance the kinetic models to describe the densification process of systems at the nanoscale.

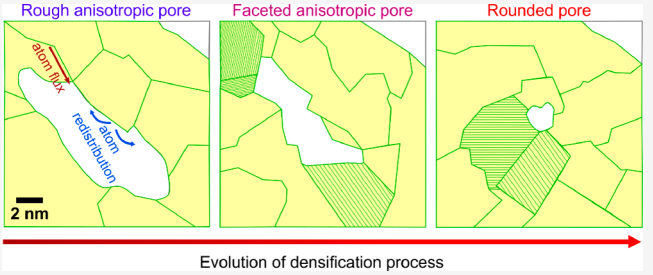

KEYWORDS: *in situ TEM, ZrO_2, nanoceramics, sintering, atom mobility*

Downloaded via UNIV FED DE SAO CARLOS on March 4, 2022 at 19:35:20 (UTC).
See https://pubs.acs.org/sharingguidelines for options on how to legitimately share published articles.

Despite being an ancient thermal process used to obtain materials, the scientific basis of the sintering process was established after the World War II.[1] The sintering is a thermally active process, where two phenomena compete for thermal energy, i.e., densification (or pore elimination) and grain growth.[1] The sintering process can be wanted, for instance, to process pore-free nanostructured materials aiming to take advantage of their grain-size dependent physical properties;[2,3] or even unwanted, particularly in nanocatalyst materials used at high temperatures.[4,5] The driving force for densification is lowering the surface free energy by replacing solid−gas interfaces. This process will result in a new, but lower-energy, solid−solid interface with a total decrease in the system's free energy.[1,6] More recently, we have witnessed significant progress in the sintering methods, which enabled us to obtain materials with differentiated properties.[1] However, getting nanostructured materials with controlled porosity and particle size is not yet a routine. The development of new synthetic routes and the controlled assembly of nanoparticles brought new hope in advancing particulate materials processing. Despite it, the use of nanoparticles to obtain nanostructured materials with controlled porosity and final grain size proved not to be an easy path. Perhaps we need to take a step back to better understand the sintering of the materials at the nanoscale (nanomaterials) and then advance in their fabrication process.

As Castro and Gouvea[7] and Cheng and Wang[8] elegantly discussed in their review articles, there are limitations in the sintering models developed for micrometric-scale particles to explain the sintering process of nanomaterials. These limitations are related to the thermodynamics driving force associated with the radius of curvature of the neck (contact area formed among particles) and the anisotropy of the surface energy of the nanoparticles.[7] In addition to the simplifications mentioned above that impact sintering models at the nanoscale, other considerations also affect kinetic models, even at the micrometric scale. For instance, the sintering models assume that atomic diffusion is the rate-controlling step for the overall sintering kinetics.[6,9] However, as Bordia et al.[1] pointed out, interfacial reactions related to atomic transport can also take part or control the sintering process. The interfacial reactions are related to faceted (atomically ordered and macroscopically straight or zig-zagged) grain boundary and pore surfaces regions.[10−13] Experimental results have indicated the existence of a critical driving force for densification in samples with faceted grain boundaries,[10−13] supporting the idea that we should consider the interfacial reaction to describe the sintering process. The correlation between the interface faceting and the limit of densification relies on the assumption that the detachment or attachment of atoms in the faceted surface can control the densification kinetics.[1,10−13] Identifying the critical driving force for the sintering process in systems that present faceted boundaries implies that the grain boundaries and pore

Received: December 6, 2021
Revised: February 23, 2022

ACS Publications © XXXX American Chemical Society

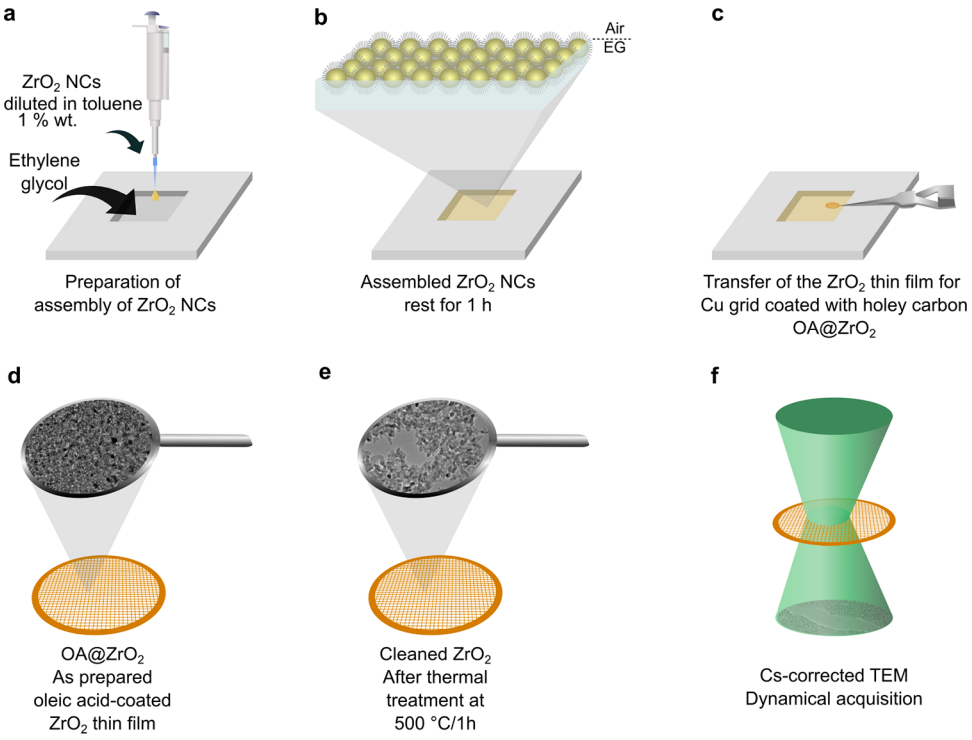

Figure 1. Schematic representation of experimental protocol. (a) OA@ZrO_2 NCs dispersed in toluene (1% wt.) were deposited on ethylene glycol (EG). (b) Assembled OA-coated ZrO_2 NCs at the EG/air interface were kept under rest for 24 h and then (c) were transferred to a holey carbon-coated Cu grid, (d) producing a continuous ZrO_2 thin film (OA@ZrO_2 thin film). (e) The grid was thermally treated at 500 °C/1 h under vacuum to remove the OA, producing a sintered and cleaned free-standing ZrO_2 thin film. (f) After the cleaning step, the grid was transferred to a Cs-corrected TEM microscope to perform the in situ analysis (electron beam current density (EBCD) of 62500 e A^{-2} s^{-1}).

surfaces are not perfect sources and sinks of atoms, without an energy barrier for the attachment/detachment of atoms.[10] Thus, further study is needed to understand the sintering kinetics in faceted systems.

In situ characterization techniques with atomic resolution based on high-resolution transmission electron microscopy (HRTEM) analysis have been used to study sintering successfully. In particular, it is possible to mention the studies about the assembly of nanoparticles deposited in a membrane and diffusional processes in nanostructured ceramic materials and metallic nanoparticles.[14−19] With the development of a proper sample preparation process, the in situ HRTEM can be a powerful tool to shed light on the study of the final stage of the sintering process with atomic resolution. Here, we report the in situ study of the sintering phenomenon at the atomic scale in ceramics formed by nanometric grains (<5 nm) of monoclinic zirconium oxide (*m*-ZrO_2). More specifically, we studied the pore elimination process in the final sintering stage (isolated pores located at the grain boundaries). The choice of ZrO_2 NCs was due to their stability in the face of oxidation state variation and radiation damage, well-known chemical and physical properties, and well-established synthesis and assembly protocols.[20] In addition, ZrO_2 is a widely employed material for different applications, such as catalysts,[21−28] composites for light-emitting diodes,[29,30] water purification,[31] Li-ion batteries,[32,33] and biomedical applications.[34−36] We used HRTEM analysis operating at room temperature in free-standing films formed by a monolayer of nanoparticles (without a supporting membrane). By joining the optimized sample preparation, the cleaning protocol, and the constant electron beam illumination, we achieved a sufficient dynamic process, allowing us to visualize the sintering process using a simple single tilt sample holder with very high spatial and temporal resolution.

The use of self-supporting (or free-standing) thin films of nanocrystals—with controlled thickness—is an alternative approach we can use to study the evolution of nanomaterials by in situ HRTEM analysis. We had used this approach to follow the in situ desintering and mechanical stability of ZrO_2 nanowires with atomic resolution.[37] We showed that in some regions of the samples, the film suffered tensile stresses due to heterogeneous densification originating from the heterogeneous packing of the ZrO_2 nanocrystals.[37] These conditions provided the perfect scenario to induce the desintering of ZrO_2 nanocrystalline bridges formed between denser regions of the sample.[38] However, we observed in other regions—under the same experimental conditions, including in the same sample—that the tensile stress seems negligible (no increase or decrease was observed in the distance between two dense regions), and the pores shrink until complete elimination. So, here we will use a similar methodology to study further the final stage of the sintering process.

We prepared the unsupported ZrO_2 film for this study by assembling oleic acid (OA)-capped monoclinic-ZrO_2 nanocrystals (OA@ZrO_2 NCs). Synthesis and morphology details about the OA@ZrO_2 NC are described in sections S1.1a and S1.2 (Figure S1a-b) of Supporting Information (SI). Here, we prepared the free-standing films directly onto the TEM Cu grid (#400) using a transfer technique. For this, we deposited a drop of OA@ZrO_2 NCs dispersed in toluene over the surface of a hydrophilic polar liquid (ethylene glycol). Due to the nonpolar (hydrophobic) nature of the OA@ZrO_2 NCs dispersion, we notice the formation of a film at the liquid−gas interface. After the toluene evaporation, a film of OA@ZrO_2 NCs is formed on

https://doi.org/10.1021/acs.nanolett.1c04708
Nano Lett. XXXX, XXX, XXX−XXX

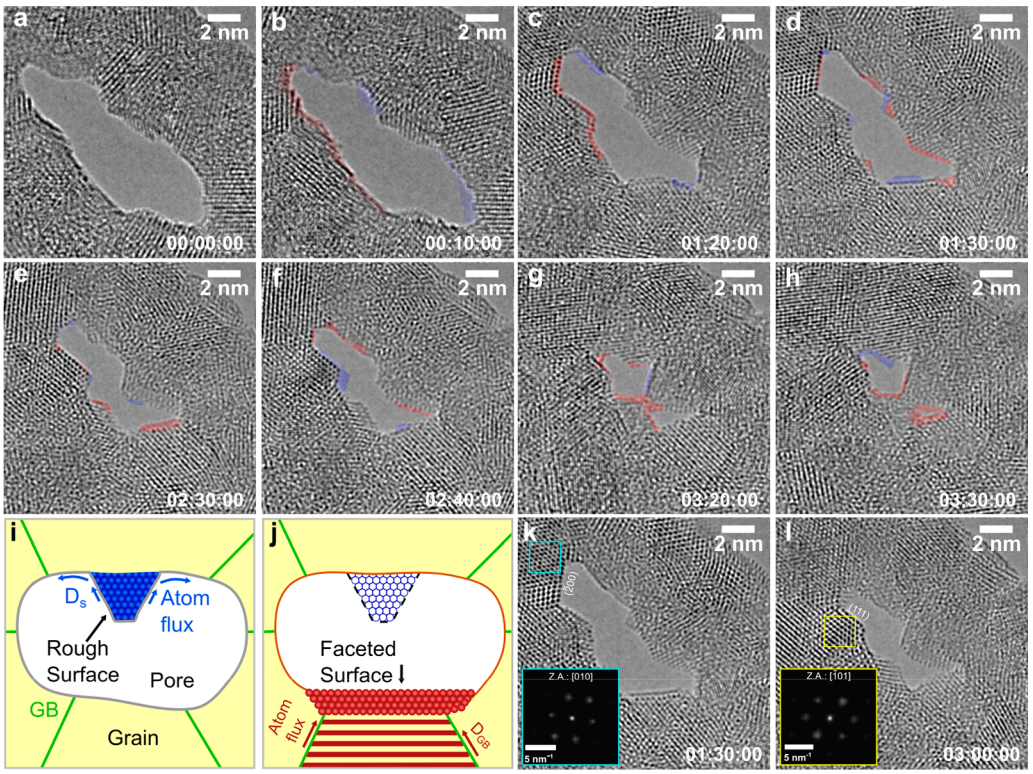

Figure 2. Evolution of Pore 1 as a function of time. (a–h) HRTEM images taken at different times, showing the pore shrinkage, highlighting the mass transport. The red regions indicate the atom addition, and the blue areas indicate atom redistribution. To properly indicate the regions of redistribution and addition of atoms, we subtract the next image from the previous one. In (g), the preferential growth in some regions led to the formation of two smaller pores with different sizes. (i,j) Schematic representation of the mass transport during the pore elimination. In (i), the rough surface (blue atoms) is redistributed in the solid–gas surface by surface diffusion (D_s). The blue arrows indicate the atom flux direction. In (j), the dashed black line indicates the initial surface that was redistributed, as well as the unfilled circles. The red outline corresponds to the new pore surface. The striped grain indicates the orientation of the grain, and the red area shows the atom attached to the faceted surface. The red arrows indicate the atom flux by the grain boundary diffusion (D_{GB}). (k,l) HRTEM images collected after 1.5 and 3 h of experiment. The insets are the FFT obtained in the highlighted squares in each image. In (k), the atom attachment occurs in the (−200) facet, then (l) the atom attachment occurs in (111) facet.

the surface of the ethylene glycol. Then, we transfer this film to the TEM Cu grid. To eliminate the organic layer of OA, we used a heat treatment in a vacuum oven (500 °C/30 min). Based on thermogravimetric analysis (see Figure S2 in the SI), complete OA elimination occurs at a temperature high than 530 °C (at atmospheric pressure). However, we did OA remotion under a vacuum of ∼1 × 10^{-2} Torr. Considering the Clausius–Clapeyron equation and the ΔH of vaporization of the OA (83.8 kJ mol^{-1}), we can estimate that (under the pressure of 1 × 10^{-2} Torr) the OA elimination (by evaporation) occurs at a temperature of ∼140 °C. Thus, at 500 °C under vacuum (∼1 × 10^{-2} Torr), we guarantee the complete elimination of OA without carbon residue. This procedure allowed us to obtain large areas of the homogeneous cleaned ZrO_2 film. After heat treatment, no phase transformation was observed, keeping the monoclinic ZrO_2 phase, as illustrated in Figure S3. Finally, the grid was transferred to a spherical aberration (Cs)-corrected FEI Titan Cubed Themis microscope to perform the analysis by HRTEM (see detail in section S1.1b in the SI). Figure 1 shows the schematic representation of the experimental procedure we used to prepare the ZrO_2 nonsupported film for the sintering study.

In our previous work using a similar methodology for the in situ TEM analysis, we observed that the electron beam (e-beam) does not cause permanent damage in our experimental conditions.[37] However, the e-beam increases surface diffusion, giving atomic mobility even at room temperature. This increase in superficial atomic mobility is well documented in the literature on nanomaterials, especially in nanocrystals without a protective organic layer.[17−19] The e-beam induced diffusion process we observed here can be associated with different effects, such as knock-on, radiolysis, damage by induced electrical field (DIEF), and electron beam heating.[39]

We calculated the e-beam induced heating considering the HRTEM experimental setup and ZrO_2 thermal conductivity (κ) of 2 W m^{-1} K^{-1}. According to the Reimer model,[40] it is possible to estimate that the rising temperature (ΔT) is around 1 K. Even considering a lower thermal conductivity (κ ranging from 0.1 to 1 W m^{-1} K^{-1}[41]) associated with the ZrO_2 NCs, the e-beam induced ΔT is in the range of 2–6 K. Then, we can neglect the e-beam induced heating during the in situ HRTEM experiments. Moreover, we believe radiolysis is less likely because this kind of damage preferentially generates point defects,[39] and in our experiment, we observed only collective atomic displacement phenomena. Another probable effect is the DIEF. However, this type of damage only occurs in extremely intense e-beam (TEM operation mode).[39] We performed the experiments under low to moderate electron beam intensity conditions.

On the other hand, knock-on is a plausible hypothesis to explain atomic mobility. We can find several articles in the literature correlating atomic mobility on transition metal oxide surfaces with the creation of vacancies (mainly oxygen vacancy) caused by a knock-on.[39] In most cases, the authors mention the formation of oxygen vacancies without a phase transformation

https://doi.org/10.1021/acs.nanolett.1c04708
Nano Lett. XXXX, XXX, XXX−XXX

or extensive beam-induced damage on the oxides. The ZrO_2 is a less reducible oxide in comparison with those reported in the literature;[42−44] thus, we could expect that the oxygen removal should be less extensive (or even reversible or in equilibrium with the amount of oxygen present in the TEM chamber), but enough to promote the atom mobility in our experimental conditions. Thus, based on these arguments, we decided to conduct the pore closure experiments in the final sintering stage at room temperature.

We follow the sintering process of two types of pores, the first (Pore 1) formed by several grain boundaries (a pore coordinated by several grains), and the second one (Pore 2) located between two grains. Figure 2 describes the temporal evolution of Pore 1. The first information we notice is that the process required hours of data collection (~6 h of continuous HRTEM analysis) to follow the entire process. Due to this, we take images in HRTEM mode every 10 min (see the complete sequence in Figure S4 in SI). The HRTEM images of Figure 2a−h illustrate representative HRTEM images of the sintering process. In these images, the regions marked in red represent where the deposition of atoms occurred, and the areas highlighted in blue represent the region where the removal of atoms occurred.

The HRTEM images displayed in Figure 2a−f clearly show that atoms are detached from the rough (atomically disordered and macroscopically rounded) surface and redistributed (by surface diffusion - D_S) in the solid−gas interface, as illustrated pictorially in Figure 2i. On the other hand, we notice that the faceted surfaces (ordered - lower energy surface) are associated with the atom's attachment process, followed by a pore area reduction. Since a pore area reduction occurs (i.e., a densification process), the atom flux must be via the grain boundary (solid−solid interface) to the pore surface (by grain boundary diffusion process; see Figure 2j). This phenomenon described before can be interpreted as a transition from a rough to a faceted surface.

The sequence of HRTEM images pictured in Figure 2a−f also shows that the atomic transport process, which induces the pore elimination, is not isotropic. We can observe (see Figure 2c, for instance) that the attachment of atoms does not occur on every pore surface but only on specific solid−gas interfaces. This anisotropic growth must be related to the surface energy anisotropy and the grain boundary diffusion coefficient (D_{GB}) anisotropy. In other words, it is a direct consequence of the different surface energies present in the solid−gas and solid−solid interfaces. This surface energy anisotropy leads to preferential growth in some regions (Figure 2e−g), leading to the formation of two pores of different sizes (Figure 2 g,h).

We can visualize the dependence of pore elimination with the surface orientation in the HRTEM images illustrated in Figure 2k,l. The inset of Figure 2k shows the FFT analysis of the region indicated by the cyan square. We can see that this grain is oriented along the zone axis [010], making it possible to identify the (−200) facet. Following the densification process, we observed the attachment of atoms along other orientations. More specifically, after 3 h, the atom's attachment occurs along the face (111), as indicated in Figure 2l (see inset with the FFT analysis, showing that the grown region is oriented along the zone axis $[\bar{1}01]$). Sojka and coauthors[45] investigated the surface energy of monoclinic ZrO_2 nanocrystals (through periodic density functional theory (DFT) calculations and atomistic thermodynamic modeling). The results showed that the surface energies of the relaxed facets increase in the following order, considering the family planes: {111} < {110} < {100}. Thus, we can observe that the pore elimination follows a tendency to eliminate the faces of higher energy.

Considering that the variation of area (A) scales with the pore volume (V) variation, and assuming the final stage of sintering is a diffusion process controlled by grain boundary diffusion, we can write that[9]

$$\frac{dA}{dt} \propto \frac{dV}{dt} \propto -\frac{K}{G^4RT} \quad (1)$$

where K is a constant (dependent on surface energy, D_{GB}, molar volume, grain boundary thickness, and geometric constants), G is the mean grain size, R is the gas constant, and T is the temperature. At a constant temperature, we find that (dA/dt) is constant (a rate of ~0.2 nm^2/min), consistent with the pore area's linear dependence as a function of time reported in Figure 3a. After the formation of the two pores (with different sizes, labeled as Pore "a" and Pore "b") around 200 min of the analysis, the densification kinetics change, leading to a modification of the slope of the curve (~0.04 nm^2/min), which is expected since variation in surface energy and other geometric parameters must occur. It is highlighted in Figure 3b.

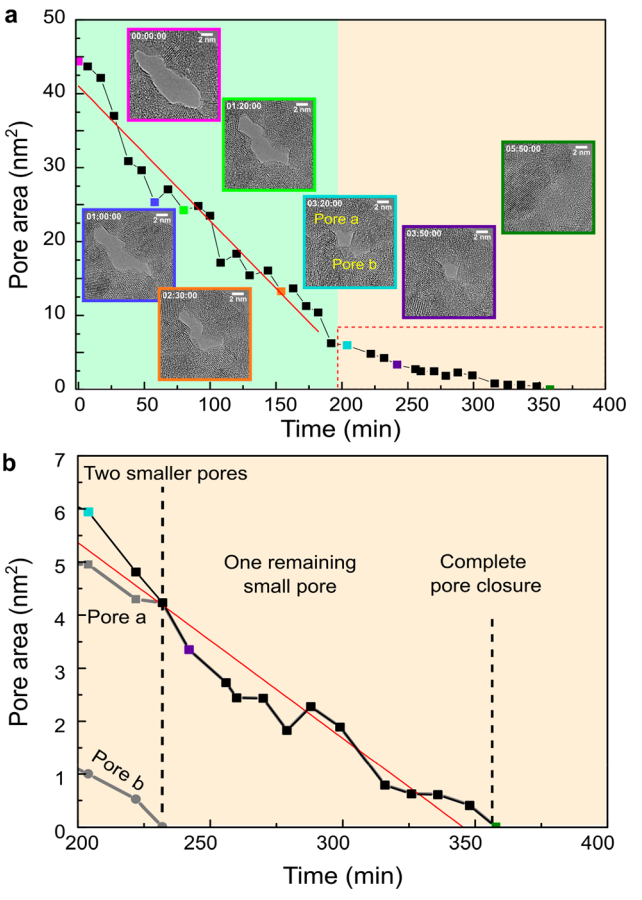

Figure 3. (a) Plot of the area of Pore 1 as a function of the time, showing a linear dependence. The x-axis was plotted in min instead of h to facilitate the visualization. The colored square in the graphic indicates the corresponding HRTEM images outlined by the same color. Scale bar: 2 nm. Around 200 min (highlighted by the yellow background), Pore 1 is partially closed, forming two smaller ones (pores a and b), as indicated in the HRTEM image outlined by cyan square. (b) Detailed plot of the pore area as a function for t > 200 min. After the formation of the smaller pores, there is a modification of the slope of the curve.

https://doi.org/10.1021/acs.nanolett.1c04708
Nano Lett. XXXX, XXX, XXX−XXX

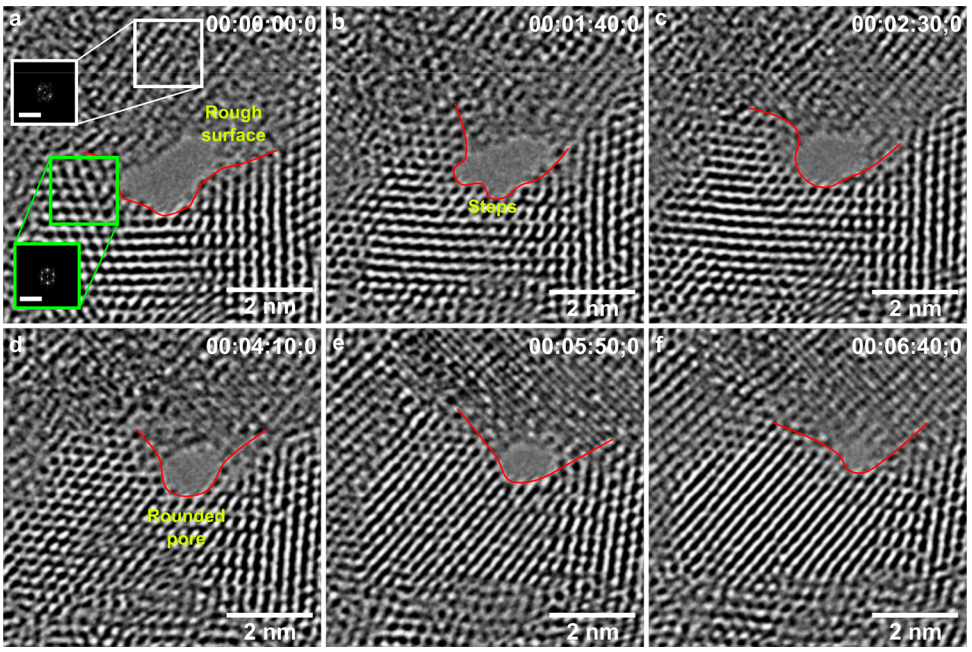

Figure 4. Direct visualization of pore shrinkage and elimination. Snapshots from Videos S1−S4 at different times, as indicated in each image. The red line indicates the grain boundary (GB) around the pore. Scale bar: 2 nm. In (a), the white and green squares indicate grains with different zone axis, as shown by the fast Fourier Transform in the insets. Scale bar of FFT: 10 nm^{-1}. In (b), the pore remained irregular, and the pore area decreased compared with (a). In (c) to (f), the pore area decreases gradually, and the pore becomes rounded.

In a different data collection, we analyzed a pore between two grains (Pore 2), taking HRTEM images at each 0.2 s (see Videos S1−S4, resulting from this data collection until complete pore elimination). We can observe in Videos S1−S4 a constant mass transport toward the pore, and in a first look, the atoms migrate from adjacent grains to the rough surface, being redistributed around the pore. We also observed the attachment of atoms to the ordered grain, filling the atomic columns. Figure 4 presents snapshots of HRTEM images obtained from Videos S1−S4 to highlight details observed in the in situ experiment.

As we can see in Figure 4a, the pore is in a high angle grain boundary, as indicated by the fast Fourier transform analysis (FFT) shown in the insets. In this type of pore, we also observed faceted solid−gas interfaces (Figure 4c,d), but what most catches our attention is the change in the pore shape. We observed that the irregular shape of the pore becomes more symmetrical with time (Figure 4a−f). This rounding of the pore shape must be a consequence of the existence of a single grain boundary (resulting in a single solid−solid interfacial energy and D_{GB}) and only two solid−gas interfaces. It seems to be associated with the lower anisotropy of surface energies when compared to the pore formed by several grain boundaries.

Our in situ experiment allows us to analyze the mobility of the grain boundary and the interaction between the grain boundary and the pore. Due to the low atomic mobility at room temperature, the force exerted by the grain boundary on the pore is not enough to drag it along, which means that the pore is coupled to the boundary during the entire sintering process (see Videos S1−S4 and Figure 4). Furthermore, we observed a reduction in the grain boundary mobility due to the presence of the pore, as suggested by the bent-over line of the grain boundary (as highlighted by the red line in Figure 4a−f), which indicates the pinning effect of the grain boundary caused by the pore. With the reduction in pore size, the grain boundary becomes less curved, as illustrated in Figure 4f.

The densification of ceramics has been widely discussed in the literature.[6,9] Looking in detail at a pore elimination in a nanostructured material, we found evidence of a very complex process strongly dependent on the surface energy gradient. Despite limiting step that dominates the kinetics depending on the system and experimental conditions, our experiment provides meaningful insights about the final stage of the sintering process for nanostructured ceramics with faceted surfaces. The use of the in situ TEM technique is nothing new in the study of the sintering processes for nanoceramics and catalysts materials;[14−19,46] however, to the best of our knowledge, no work has shown the pore elimination process with an atomic resolution like the one presented here. The study of mass transport processes involving microstructural evolution, with the nanometric or atomic resolution, was only possible so far via computational simulation based on molecular dynamics.[47−49] Here, with the development of an innovative sample preparation technique and with the use of ZrO_2 nanocrystals with a size smaller than 5 nm, we followed the temporal evolution of the sintering phenomena with atomic resolution. Our results show that, during the densification process, the solid−gas interface undergoes a transition process from a rough surface to a faceted surface. This type of transition was reported for solid−solid interfaces (grain boundaries) in metallic and ceramic systems during the sintering and grain growth process.[50] However, despite theoretical predictions and experimental evidence,[11,12,50,51] such a transition has never been reported in a densification process, especially in situ and with atomic resolution. The transition from a rough surface to a faceted surface described here is not a surface reconstruction process. We observed that the rough surface disappears and the faceted surface originates from an atom attachment process which leads to a reduction in the pore area (i.e., a densifying process). This surface transition is anisotropic concerning crystallographic orientation and therefore surface energy. The fact that there are

https://doi.org/10.1021/acs.nanolett.1c04708
Nano Lett. XXXX, XXX, XXX−XXX

preferential solid−gas interfaces for the attachment/detachment of atoms strongly suggests that the GB and pore surfaces are not perfect sources and sinks of atoms. Thus, our discovery supports the existence of a critical driving force for the attachment/detachment of atoms in nanometric ceramics, suggesting that interfacial reactions related to atomic transportation can also take part or control the sintering process.[1,10]

Another result reported here is the influence of the surface energy anisotropy on the densification process. It was clear that this anisotropy leads to non-isotropic mass transportation during the elimination of the pore coordinated by several grains. One consequence of our discovery is that this anisotropy takes an important role in densification. The surface energy difference, considering the difference between surfaces with different crystallographic orientations and the energy difference between the surface and the grain boundary, can be considered an additional driving force for the pore elimination process, as pointed out by Castro and Gouvea.[7] Finally, we show that pores in nanoceramics also act as pinning to reduce the mobility of the grain boundary, as already predicted in micrometric ceramics.[1,52,53]

Thus, considering future development, we would like to suggest two energetics terms to be incorporated in the densification sintering models of nanoceramics. The first term must considerer the difference between the grain boundary energy (γ_{GB}) and surface energy (γ_{SV}). The second term must consider the energy associated with the detachment of atoms at grain boundary and surface atom attachment. This second term may be associated with a thermodynamic barrier related to chemical bond energy.

In summary, the results reported here provide new insights, contributing to a better understanding of the sintering process in nanoceramics. Our findings certainly can contribute to the development of improved kinetic models to describe the densification process of nanomaterials. We believe that the results shown here will also contribute to the development of dense nanoceramics.

■ ASSOCIATED CONTENT

Supporting Information

The Supporting Information is available free of charge at https://pubs.acs.org/doi/10.1021/acs.nanolett.1c04708.

Detailed experimental procedures; results and additional discussion (PDF)

Pore elimination as a function of the time (AVI)

Pore elimination as a function of the time (AVI)

Pore elimination as a function of the time (AVI)

Pore elimination as a function of the time (AVI)

■ AUTHOR INFORMATION

Corresponding Author

Edson Roberto Leite − *Laboratório Nacional de Nanotecnologia (LNNano), CNPEM, 13083-970 Campinas, São Paulo, Brazil; Departamento de Química, Universidade Federal de São Carlos, 13565-905 São Carlos, São Paulo, Brazil;* orcid.org/0000-0002-0513-9939; Email: edson.leite@lnnano.cnpem.br

Authors

Tanna Elyn Rodrigues Fiuza − *Laboratório Nacional de Nanotecnologia (LNNano), CNPEM, 13083-970 Campinas, São Paulo, Brazil;* orcid.org/0000-0001-7841-2521

Marlon Muniz da Silva − *Laboratório Nacional de Nanotecnologia (LNNano), CNPEM, 13083-970 Campinas, São Paulo, Brazil; Faculdade de Química, Centro de Ciências Exatas, Ambientais e de Tecnologias (CEATEC), Pontifícia Universidade Católica de Campinas (PUCCamp), 13086-900 Campinas, São Paulo, Brazil*

Jefferson Bettini − *Laboratório Nacional de Nanotecnologia (LNNano), CNPEM, 13083-970 Campinas, São Paulo, Brazil*

Complete contact information is available at: https://pubs.acs.org/10.1021/acs.nanolett.1c04708

Author Contributions

T.E.R.F. performed HRTEM measurements, data process, data analysis, and manuscript preparation. M.M.S performed and optimized the ZrO_2 film preparation and cleaning. J.B. contributed to the data process, data analysis, and manuscript preparation. E.R.L. contributed to the design of HRTEM experiments, supervised the data process and data analysis, and manuscript preparation.

Notes

The authors declare no competing financial interest.

■ ACKNOWLEDGMENTS

São Paulo Research Foundation (FAPESP) grant number: CEPID 2013/07296-2. National Council for Scientific and Technological Development (CNPq) grant number 380866/2020-0.

■ REFERENCES

(1) Bordia, R. K.; Kang, S. L.; Olevsky, E. A. Current Understanding and Future Research Directions at the Onset of the next Century of Sintering Science and Technology. *J. Am. Ceram. Soc.* **2017**, *100* (6), 2314−2352.

(2) Gong, Z.; Zhao, W.; Guan, K.; Rao, P.; Zeng, Q.; Liu, J.; Feng, Z. Influence of Grain Boundary and Grain Size on the Mechanical Properties of Polycrystalline Ceramics: Grain-scale Simulations. *J. Am. Ceram. Soc.* **2020**, *103* (10), 5900−5913.

(3) Wollmershauser, J. A.; Feigelson, B. N.; Gorzkowski, E. P.; Ellis, C. T.; Goswami, R.; Qadri, S. B.; Tischler, J. G.; Kub, F. J.; Everett, R. K. An Extended Hardness Limit in Bulk Nanoceramics. *Acta Mater.* **2014**, *69*, 9−16.

(4) Mitchell, S.; Qin, R.; Zheng, N.; Pérez-Ramírez, J. Nanoscale Engineering of Catalytic Materials for Sustainable Technologies. *Nat. Nanotechnol.* **2021**, *16* (2), 129−139.

(5) Cao, A.; Lu, R.; Veser, G. Stabilizing Metal Nanoparticles for Heterogeneous Catalysis. *Phys. Chem. Chem. Phys.* **2010**, *12* (41), 13499.

(6) Rahaman, M. N. *Sintering of Ceramics*; CRC Press, 2007.

(7) Castro, R. H. R.; Gouvêa, D. Sintering and Nanostability: The Thermodynamic Perspective. *J. Am. Ceram. Soc.* **2016**, *99* (4), 1105−1121.

(8) Chen, I.-W.; Wang, X. Sintering of Nanograin Ceramics. In *Ceramics Science and Technology*, Riedel, R.; Chen, I., Eds.; Wiley-VCH Verlag GmbH & Co. KGaA, 2012; pp 441−455.

(9) Kang, S.-J. L. Grain Boundary Energy and Sintering. In *Sintering: Densification, Grain Growth and Microstructure*, Kang, S.-J. L., Ed.; Elsevier Butterworth-Heinemann, Oxford, 2004; pp 139−143.

(10) Kang, K.-S. J. Sintering. In *Ceramics Science and Technology*, Riedel, R.; Chen, I., Eds.; Wiley-VCH Verlag & Co. KGaA, Weinheim, 2012; pp 141−169.

(11) Choi, S.-Y.; Kang, S.-J. L. Sintering Kinetics by Structural Transition at Grain Boundaries in Barium Titanate. *Acta Mater.* **2004**, *52* (10), 2937−2943.

(12) Lee, M.-G.; Chung, S.-Y.; Kang, S.-J. L. Boundary Faceting-Dependent Densification in a $BaTiO_3$ Model System. *Acta Mater.* **2011**, *59* (2), 692−698.
(13) An, S.-M.; Yoon, B.-K.; Chung, S.-Y.; Kang, S.-J. L. Nonlinear Driving Force−Velocity Relationship for the Migration of Faceted Boundaries. *Acta Mater.* **2012**, *60* (11), 4531−4539.
(14) Rankin, J. In Situ TEM Heating of Nanosized ZrO_2. *J. Am. Ceram. Soc.* **1999**, *82* (6), 1560−1564.
(15) Phuah, X. L.; Jian, J.; Wang, H. H.; Wang, X.; Zhang, X.; Wang, H. H. Ultra-High Heating Rate Effects on the Sintering of Ceramic Nanoparticles: An in Situ TEM Study. *Mater. Res. Lett.* **2021**, *9* (9), 373−381.
(16) Podor, R.; Trillaud, V.; Nkou Bouala, G. I.; Dacheux, N.; Ricolleau, C.; Clavier, N. A Multiscale in Situ High Temperature High Resolution Transmission Electron Microscopy Study of ThO_2 Sintering. *Nanoscale* **2021**, *13* (15), 7362−7374.
(17) van Huis, M. A.; Kunneman, L. T.; Overgaag, K.; Xu, Q.; Pandraud, G.; Zandbergen, H. W.; Vanmaekelbergh, D. Low-Temperature Nanocrystal Unification through Rotations and Relaxations Probed by in Situ Transmission Electron Microscopy. *Nano Lett.* **2008**, *8* (11), 3959−3963.
(18) Lim, T. H.; McCarthy, D.; Hendy, S. C.; Stevens, K. J.; Brown, S. A.; Tilley, R. D. Real-Time TEM and Kinetic Monte Carlo Studies of the Coalescence of Decahedral Gold Nanoparticles. *ACS Nano* **2009**, *3* (11), 3809−3813.
(19) Wu, J.; Gao, W.; Wen, J.; Miller, D. J.; Lu, P.; Zuo, J.-M.; Yang, H. Growth of Au on Pt Icosahedral Nanoparticles Revealed by Low-Dose In Situ TEM. *Nano Lett.* **2015**, *15* (4), 2711−2715.
(20) Dalmaschio, C. J.; Da Silveira Firmiano, E. G.; Pinheiro, A. N.; Sobrinho, D. G.; Farias De Moura, A.; Leite, E. R. Nanocrystals Self-Assembled in Superlattices Directed by the Solvent-Organic Capping Interaction. *Nanoscale* **2013**, *5* (12), 5602−5610.
(21) Zhou, C.; Shi, J.; Zhou, W.; Cheng, K.; Zhang, Q.; Kang, J.; Wang, Y. Highly Active ZnO-ZrO_2 Aerogels Integrated with H-ZSM-5 for Aromatics Synthesis from Carbon Dioxide. *ACS Catal.* **2020**, *10* (1), 302−310.
(22) Li, K.; Chen, J. G. CO_2 Hydrogenation to Methanol over ZrO_2-Containing Catalysts: Insights into ZrO_2 Induced Synergy. *ACS Catal.* **2019**, *9* (9), 7840−7861.
(23) Tada, S.; Katagiri, A.; Kiyota, K.; Honma, T.; Kamei, H.; Nariyuki, A.; Uchida, S.; Satokawa, S. Cu Species Incorporated into Amorphous ZrO_2 with High Activity and Selectivity in CO_2-to-Methanol Hydrogenation. *J. Phys. Chem. C* **2018**, *122* (10), 5430−5442.
(24) Dostagir, N. H. M.; Rattanawan, R.; Gao, M.; Ota, J.; Hasegawa, J.; Asakura, K.; Fukouka, A.; Shrotri, A. Co Single Atoms in ZrO_2 with Inherent Oxygen Vacancies for Selective Hydrogenation of CO_2 to CO. *ACS Catal.* **2021**, *11* (15), 9450−9461.
(25) Wu, C.; Lin, L.; Liu, J.; Zhang, J.; Zhang, F.; Zhou, T.; Rui, N.; Yao, S.; Deng, Y.; Yang, F.; et al. Inverse ZrO_2/Cu as a Highly Efficient Methanol Synthesis Catalyst from CO_2 Hydrogenation. *Nat. Commun.* **2020**, *11* (1), 5767.
(26) Tsoukalou, A.; Abdala, P. M.; Armutlulu, A.; Willinger, E.; Fedorov, A.; Müller, C. R. *Operando* X-Ray Absorption Spectroscopy Identifies a Monoclinic ZrO_2 :In Solid Solution as the Active Phase for the Hydrogenation of CO_2 to Methanol. *ACS Catal.* **2020**, *10* (17), 10060−10067.
(27) Temvuttirojn, C.; Poo-arporn, Y.; Chanlek, N.; Cheng, C. K.; Chong, C. C.; Limtrakul, J.; Witoon, T. Role of Calcination Temperatures of ZrO_2 Support on Methanol Synthesis from CO_2 Hydrogenation at High Reaction Temperatures over ZnO_x/ZrO_2 Catalysts. *Ind. Eng. Chem. Res.* **2020**, *59* (13), 5525−5535.
(28) Tada, S.; Kayamori, S.; Honma, T.; Kamei, H.; Nariyuki, A.; Kon, K.; Toyao, T.; Shimizu, K.; Satokawa, S. Design of Interfacial Sites between Cu and Amorphous ZrO_2 Dedicated to CO_2-to-Methanol Hydrogenation. *ACS Catal.* **2018**, *8* (9), 7809−7819.
(29) Liu, H.; Tan, Y.; Cao, M.; Hu, H.; Wu, L.; Yu, X.; Wang, L.; Sun, B.; Zhang, Q. Fabricating $CsPbX_3$-Based Type I and Type II Heterostructures by Tuning the Halide Composition of Janus $CsPbX_3$/ZrO_2 Nanocrystals. *ACS Nano* **2019**, *13* (5), 5366−5374.
(30) Duan, Y.; Ezquerro, C.; Serrano, E.; Lalinde, E.; García-Martínez, J.; Berenguer, J. R.; Costa, R. D. Meeting High Stability and Efficiency in Hybrid Light-Emitting Diodes Based on SiO_2/ZrO_2 Coated $CsPbBr_3$ Perovskite Nanocrystals. *Adv. Funct. Mater.* **2020**, *30* (40), 2005401.
(31) Chen, Y.; Yang, G.; Liu, B.; Kong, H.; Xiong, Z.; Guo, L.; Wei, G. Biomineralization of ZrO_2 Nanoparticles on Graphene Oxide-Supported Peptide/Cellulose Binary Nanofibrous Membranes for High-Performance Removal of Fluoride Ions. *Chem. Eng. J.* **2022**, *430*, 132721.
(32) Khalili Azar, M.; Razmjoo Khollari, M. A.; Esmaeili, M.; Heidari, E.; Hosseini-Hosseinabad, S. M.; Siavash Moakhar, R.; Dolati, A.; Ramakrishna, S. Enhanced Electrochemical Performance and Thermal Stability of ZrO_2 - and RGO−ZrO_2 -Coated $Li[Ni_{0.8}Co_{0.1}Mn_{0.1}]O_2$ Cathode Material for Li-Ion Batteries. *ACS Appl. Energy Mater.* **2021**, *4* (1), 934−945.
(33) Schipper, F.; Bouzaglo, H.; Dixit, M.; Erickson, E. M.; Weigel, T.; Talianker, M.; Grinblat, J.; Burstein, L.; Schmidt, M.; Lampert, J.; et al. From Surface ZrO_2 Coating to Bulk Zr Doping by High Temperature Annealing of Nickel-Rich Lithiated Oxides and Their Enhanced Electrochemical Performance in Lithium Ion Batteries. *Adv. Energy Mater.* **2018**, *8* (4), 1701682.
(34) Srigurunathan, K.; Meenambal, R.; Guleria, A.; Kumar, D.; Ferreira, J. M. d. F.; Kannan, S. Unveiling the Effects of Rare-Earth Substitutions on the Structure, Mechanical, Optical, and Imaging Features of ZrO_2 for Biomedical Applications. *ACS Biomater. Sci. Eng.* **2019**, *5* (4), 1725−1743.
(35) Su, L.; Wu, Q.; Tan, L.; Huang, Z.; Fu, C.; Ren, X.; Xia, N.; Chen, Z.; Ma, X.; Lan, X.; et al. High Biocompatible ZIF-8 Coated by ZrO_2 for Chemo-Microwave Thermal Tumor Synergistic Therapy. *ACS Appl. Mater. Interfaces* **2019**, *11* (11), 10520−10531.
(36) Isacfranklin, M.; Dawoud, T.; Ameen, F.; Ravi, G.; Yuvakkumar, R.; Kumar, P.; Hong, S. I.; Velauthapillai, D.; Saravanakumar, B. Synthesis of Highly Active Biocompatible ZrO_2 Nanorods Using a Bioextract. *Ceram. Int.* **2020**, *46* (16), 25915−25920.
(37) Focassio, B.; Fiuza, T. E. R.; Bettini, J.; Schleder, G. R.; Rodrigues, M. H. M.; Junior, J. B. S.; Fazzio, A.; Capaz, R. B.; Leite, E. R. Stability and Rupture of an Ultrathin Ionic Wire. *Submitted*.
(38) Lange, F. F. De-Sintering, A Phenomenon Concurrent with Densification within Powder Compacts: A Review. In *Sintering Technology*, German, R. M.; Messing, G. L.; Cornwall, R. G., Eds.; Marcel Dekker Inc: New York, 1996; pp 1−12.
(39) Jiang, N. Electron Beam Damage in Oxides: A Review. *Rep. Prog. Phys.* **2016**, *79* (1), 016501.
(40) Reimer, L.; Kohl, H. *Transmission Electron Microscopy*; Springer Series in Optical Sciences; Springer New York: New York, NY, 2008; Vol. *36*. DOI: 10.1007/978-0-387-40093-8.
(41) Yang, H.-S.; Bai, G.-R.; Thompson, L. J.; Eastman, J. A. Interfacial Thermal Resistance in Nanocrystalline Yttria-Stabilized Zirconia. *Acta Mater.* **2002**, *50* (9), 2309−2317.
(42) Sundararajan, J. A.; Kaur, M.; Qiang, Y. Mechanism of Electron Beam Induced Oxide Layer Thickening on Iron−Iron Oxide Core−Shell Nanoparticles. *J. Phys. Chem. C* **2015**, *119* (15), 8357−8363.
(43) Lawrence, E. L.; Levin, B. D. A.; Miller, B. K.; Crozier, P. A. Approaches to Exploring Spatio-Temporal Surface Dynamics in Nanoparticles with in Situ Transmission Electron Microscopy. *Microsc. Microanal.* **2020**, *26*, 86−94.
(44) Bugnet, M.; Overbury, S. H.; Wu, Z. L.; Epicier, T. Direct Visualization and Control of Atomic Mobility at {100} Surfaces of Ceria in the Environmental Transmission Electron Microscope. *Nano Lett.* **2017**, *17* (12), 7652−7658.
(45) Piskorz, W.; Gryboś, J.; Zasada, F.; Cristol, S.; Paul, J.-F.; Adamski, A.; Sojka, Z. Periodic DFT and Atomistic Thermodynamic Modeling of the Surface Hydration Equilibria and Morphology of Monoclinic ZrO_2 Nanocrystals. *J. Phys. Chem. C* **2011**, *115* (49), 24274−24286.

https://doi.org/10.1021/acs.nanolett.1c04708
Nano Lett. XXXX, XXX, XXX−XXX

(46) Hansen, T. W.; DeLaRiva, A. T.; Challa, S. R.; Datye, A. K. Sintering of Catalytic Nanoparticles: Particle Migration or Ostwald Ripening? *Acc. Chem. Res.* **2013**, *46* (8), 1720−1730.
(47) Jensen, P. Growth of Nanostructures by Cluster Deposition: Experiments and Simple Models. *Rev. Mod. Phys.* **1999**, *71* (5), 1695−1735.
(48) McCarthy, D. N.; Brown, S. A. Evolution of Neck Radius and Relaxation of Coalescing Nanoparticles. *Phys. Rev. B* **2009**, *80* (6), 064107.
(49) Lai, K. C.; Evans, J. W. Reshaping and Sintering of 3D Fcc Metal Nanoclusters: Stochastic Atomistic Modeling with Realistic Surface Diffusion Kinetics. *Phys. Rev. Mater.* **2019**, *3* (2), 026001.
(50) Straumal, B. B.; Kogtenkova, O. A.; Gornakova, A. S.; Sursaeva, V. G.; Baretzky, B. Review: Grain Boundary Faceting−Roughening Phenomena. *J. Mater. Sci.* **2016**, *51* (1), 382−404.
(51) Pontikis, V.; Sindzingre, P. Surface Melting and Roughening Transition. *Phys. Scr.* **1987**, *T19B*, 375−381.
(52) Brook, R. J. Pore-Grain Boundary Interactions and Grain Growth. *J. Am. Ceram. Soc.* **1969**, *52* (1), 56−57.
(53) Hsueh, C. H.; Evans, A. G.; Coble, R. L. Microstructure Development during Final/Intermediate Stage Sintering—I. Pore/Grain Boundary Separation. *Acta Metall.* **1982**, *30* (7), 1269−1279.

https://doi.org/10.1021/acs.nanolett.1c04708
Nano Lett. XXXX, XXX, XXX−XXX